

Supporting Information

Phosphorescent Molecular Tweezers Based on Alkynylplatinum(II) Terpyridine System: Turning on of NIR Emission via Heterologous Pt···M Interaction (M = Pt^{II}, Pd^{II}, Au^{III} and Au^I)

Yuya Tanaka, Keith Man-Chung Wong and Vivian Wing-Wah Yam*

Institute of Molecular Functional Materials (Areas of Excellence Scheme, University Grants Committee, Hong Kong) and Department of Chemistry,
The University of Hong Kong, Pokfulam Road, Hong Kong

Email: wwyam@hku.hk

Fax: (852) 2857-1586, Tel: (852) 2859-2153

Experimental

Materials and Reagents

All the guest complexes, $[\text{Pt}(\text{C}^{\wedge}\text{N}^{\wedge}\text{C})(\text{C}\equiv\text{N}-\text{C}_6\text{H}_4-\text{OMe})-p]$,^[S1] $[\text{Pt}(\text{C}^{\wedge}\text{N}^{\wedge}\text{C})(\text{C}\equiv\text{C}-\text{C}_6\text{H}_4-\text{OMe})-p](\text{NBu}_4)$,^[S2] $[\text{Pt}(\text{C}^{\wedge}\text{N}^{\wedge}\text{C})(\text{DMSO})]$,^[S2] $[\text{Pt}(\text{O}^{\wedge}\text{N}^{\wedge}\text{O})\text{Cl}](\text{NBu}_4)$,^[S3] $[\text{Pt}(\text{N}5\text{C}12)\text{Cl}]\text{PF}_6$,^[S4] $[\text{Pd}(\text{N}5\text{C}12)\text{Cl}]\text{PF}_6$,^[S4] $[\text{Au}(\text{C}\equiv\text{CPh})_2](\text{PNP})$ ^[S5] and $[\text{Au}(\text{C}^{\wedge}\text{N}^{\wedge}\text{C})(\text{C}\equiv\text{C}-\text{C}_6\text{H}_4-\text{OMe})-p]$ ^[S6] were synthesized according to reported procedures. 1,3-Dibromo-5-*tert*-butylbenzene^[S7] and $[\text{Pt}(\text{tpy})\text{Cl}](\text{OTf})$ ^[S8] were prepared according to literature procedures. All solvents for syntheses were of analytical grade and were used as received.

Synthesis

3-Bromo-5-*tert*-butylphenylboronic acid. A mixture of 1,3-dibromo-5-*tert*-butylbenzene (2.00 g, 6.80 mmol) and diethyl ether (25 mL) was cooled at -78°C under a nitrogen atmosphere. To the solution mixture was added *n*-BuLi (4.25 mL, 1.6 M in hexane) in a dropwise manner and the reaction mixture was stirred at 0°C for 1 h. The solution was then re-cooled to -78°C and to it was added trimethyl borate (1.14 mL, 10.2 mmol) in one portion via a syringe. The solution was allowed to warm gradually to room temperature and stirred overnight. The reaction was quenched by HCl (3 M, 20 mL), extracted with diethyl ether and washed with deionized water and the organic layer was dried over anhydrous MgSO_4 and filtered. The filtrate was evaporated to dryness under reduced pressure and the residue was washed with hexane to give the titled compound as a white solid (605 mg, 2.35 mmol, 35 %). ^1H NMR (400 MHz, CDCl_3 , 298 K, relative to Me_4Si)/ppm: δ 1.42 (s, 18 H, *t*-Bu), 7.72 (t, $J = 1.6$ Hz, 2 H, phenyl), 8.11 (t, $J = 1.6$ Hz, 2 H, phenyl), 8.17 (t, $J = 1.6$ Hz, 2 H, phenyl). Positive EI-MS: m/z 225 $[\text{M} - 2\text{OH}]^+$, HRMS (Positive EI): m/z found (calcd for $\text{C}_{10}\text{H}_{10}^{11}\text{B}^{79}\text{Br}$), 219.9884 (220.0053).

2,6-Bis(3-bromo-5-*tert*-butylphenyl)pyridine. To a mixture of 2,6-dibromopyridine (1.20 g, 4.67 mmol), Pd(PPh₃)₄ (108 mg, 0.0934 mmol), aqueous Na₂CO₃ (3 mL, 2M), and toluene (4 mL) were added 3-bromo-5-*tert*-butylphenylboronic acid (553 mg, 2.33 mmol) and ethanol (3 mL) under a nitrogen atmosphere and the reaction mixture was heated to reflux overnight. To the solution cooled at room temperature was added deionized water, and the mixture was extracted with diethyl ether. The organic layer was dried over anhydrous MgSO₄, and filtered. The filtrate was evaporated to dryness and the residue was purified by column chromatography on silica gel using hexane to CH₂Cl₂-hexane (2:1 v/v) to give the product as a white solid (1.167 g, 2.32 mmol, 99 %). ¹H NMR (400 MHz, CDCl₃, 298 K, relative to Me₄Si)/ppm: δ 1.41 (s, 18 H, *t*-Bu), 7.60 (t, *J* = 1.6 Hz, 2 H, phenyl), 7.69 (d, *J* = 8.0 Hz, 2 H, pyridine), 7.85 (t, *J* = 8.0 Hz, 1 H, pyridine), 8.05 (t, *J* = 1.6 Hz, 2 H, phenyl), 8.18 (t, *J* = 1.6 Hz, 2 H, phenyl). Positive FAB-MS: *m/z* 502 [M + H]⁺, HRMS (Positive EI): *m/z* found (calcd for C₂₅H₂₉N), 343.2284 (343.2295).

2,6-Bis(3-trimethylsilylethynyl-5-*tert*-butylphenyl)pyridine. To a mixture of 2,6-bis(3-bromo-5-*tert*-butylphenyl)pyridine (1.206 g, 2.41 mmol), Pd(PPh₃)Cl₂ (169 mg, 0.241 mmol, 10 mol%) and CuI (66.8 mg, 0.482 mmol, 20 mol%) under an inert atmosphere of nitrogen were added NEt₃ (30 mL) and trimethylsilyl acetylene (1.02 mL, 7.21 mmol). The mixture was heated to reflux for overnight. The resultant mixture was evaporated to dryness under reduced pressure and subjected to column chromatography on silica gel using hexane and CH₂Cl₂-hexane (3:2 v/v) to give the product as a yellow oil (1.21 g, 2.27 mmol, 94 %). ¹H NMR (400 MHz, CDCl₃, 298 K, relative to Me₄Si)/ppm: δ 0.20 (s, 18 H, Me₃Si), 1.41 (s, 18 H, *t*-Bu), 7.60 (t, *J* = 1.6 Hz, 2 H, phenyl), 7.69 (d, *J* = 7.6 Hz, 2 H, pyridine), 7.85 (t, *J* = 7.6 Hz, 1 H, pyridine), 8.04 (t, *J* = 1.6 Hz, 2 H, phenyl), 8.17 (t, *J* = 1.6 Hz, 2 H, phenyl). Positive FAB-MS: *m/z*

536 [M + H]⁺, HRMS (Positive EI): *m/z* found (calcd for C₃₅H₄₅N₂₈Si), 535.3078 (535.3085).

2,6-Bis(3-ethynyl-5-*tert*-butylphenyl)pyridine. To a THF (10 mL) solution of 2,6-bis(3-trimethylsilylethynyl-5-*tert*-butylphenyl)pyridine (1.21 g, 2.27 mmol) was added a methanolic solution (20 mL) of K₂CO₃ (308 mg, 2.23 mmol) and the mixture was stirred for 2 h. The reaction was quenched by deionized water and the organic layer was extracted with ethyl acetate, washed with brine and deionized water, and dried over anhydrous MgSO₄, and filtered. The filtrate was evaporated to dryness and subjected to column chromatography on silica gel using hexane and CH₂Cl₂-hexane (1:3) as eluent to give the product as a sticky white solid (688 mg, 1.76 mmol, 78 %). ¹H NMR (400 MHz, CDCl₃, 298 K, relative to Me₄Si)/ppm: δ 1.42 (s, 18 H, *t*-Bu), 3.12 (s, 2 H, acetylene), 7.62 (t, *J* = 1.6 Hz, 2 H, phenyl), 7.71 (d, *J* = 8.0 Hz, 2 H, pyridine), 7.84 (t, *J* = 8.0 Hz, 1 H, pyridine), 8.02 (t, *J* = 1.6 Hz, 2 H, phenyl), 8.31 (t, *J* = 1.6 Hz, 2 H, phenyl). Positive FAB-MS: *m/z* 391 [M]⁺, HRMS (Positive EI): *m/z* found (calcd for C₂₉H₂₉N), 391.2284 (391.2295).

Complex 1. To a mixture of [Pt(tpy)Cl](OTf) (152 mg, 1.91 mmol), 2,6-bis(3-ethynyl-5-*tert*-butylphenyl)pyridine (35.6 mg, 0.909 mmol), and CuI (5 mg, 0.03 mmol) under an inert atmosphere of nitrogen was added a degassed CH₂Cl₂ solution (60 mL) of NEt₃ (0.8 mL) and the mixture was stirred overnight at room temperature. The solution was concentrated by evaporation under reduced pressure and the residue was subjected to column chromatography on silica gel using CH₂Cl₂ and CH₂Cl₂-acetone (1:1 v/v) as eluent to give the product as an orange solid. Recrystallization using CH₂Cl₂-diethyl ether mixture gave **1** as orange microcrystals (140 mg, 0.734 mmol, 81 %). ¹H NMR (400 MHz, CDCl₃, 298 K, relative to Me₄Si)/ppm: δ 1.45 (s, 18 H, *t*-Bu on phenyl), 1.47 (s, 36 H, *t*-Bu on pyridine), 1.57 (s,

18 H, *t*-Bu on pyridine), 7.60–7.64 (m, 6 H, H_b and H_g), 7.77 (d, $J = 7.6$ Hz, 2 H, H_h), 7.85 (t, $J = 7.6$ Hz, 1 H, H_i), 8.14 (t, 1.6 Hz, 2 H, H_f), 8.20 (t, $J = 1.6$ Hz, 2 H, H_e), 8.37 (d, $J = 1.6$ Hz, 2H, H_c), 8.42 (s, 2H, H_d), 9.17 (d with ¹⁹⁵Pt satellite, $J_{\text{HH}} = 6.0$ Hz, $J_{\text{PtH}} = 17.4$ Hz, H_a). Positive FAB-MS: m/z 1582 [M]⁺, 1732 [M + OTf]⁺. Positive ESI-MS: 791 [M]²⁺, 1731 [M + OTf]⁺. Elemental analyses calcd for C₈₅H₉₈F₆N₇O_{6.5}Pt₂S₂ (1•0.5H₂O), found (calcd): C, 53.83 (54.02); H, 5.19 (5.23); N, 5.12 (5.19).

Complex 2. This was synthesized according to a procedure similar to that of **1** except that 5 equivalents of 2,6-bis(3-trimethylsilylethynyl-5-tert-butylphenyl)pyridine to [Pt(tpy)Cl](OTf) were used instead of 1 equivalent (206 mg, 0.181 mmol, 72 %). ¹H NMR (400 MHz, CDCl₃, 298 K, relative to Me₄Si)/ppm: δ 1.41 (s, 9 H, *t*-Bu on phenyl), 1.45 (s, 9 H, *t*-Bu on phenyl), 1.51 (s, 18 H, *t*-Bu on tpy), 1.64 (s, 9 H, *t*-Bu on tpy), 3.09 (s, 1 H, acetylene), 7.59–7.65 (m, 4 H, phenyl and tpy), 7.70 (d, $J = 8.0$ Hz, 1 H, pyridine), 7.75 (d, $J = 8.0$ Hz, 1 H, pyridine), 7.84 (dd, $J_1 = J_2 = 8.0$ Hz, 1 H, pyridine), 8.04 – 8.06 (m, 2 H, phenyl), 8.22 (t, $J = 1.6$ Hz, 1 H, phenyl), 8.30 (t, $J = 1.6$ Hz, 1 H, phenyl), 8.43 (d, $J = 1.2$ Hz, 2H, tpy), 8.51 (s, 2H, tpy), 9.22 (d with ¹⁹⁵Pt satellite, $J_{\text{HH}} = 6.0$ Hz, $J_{\text{PtH}} = 18.0$ Hz). Positive FAB-MS: m/z 988 [M+H]⁺. Elemental analyses calcd for C₅₇H₆₄F₃N₄O_{3.5}PtS (2•0.5H₂O), found (calcd): C, 59.51 (59.78); H, 5.64 (5.63); N, 4.62 (4.89).

Crystal Structure Determination. Crystal data for C₈₃H₉₇N₇Pt₂(C₄H₁₀O)₂(CF₃O₃S)₂ ([1•(C₄H₁₀O)₂(CF₃O₃S)₂): fw = 2029.24, triclinic, P $\bar{1}$ (No. 2), $a = 19.5557(18)$ Å, $b = 20.1957(19)$ Å, $c = 30.683(3)$ Å, $\alpha = 99.204(1)^\circ$, $\beta = 101.673(2)^\circ$, $\gamma = 95.081(2)^\circ$, $V = 11622.5(19)$ Å³, $Z = 4$, $D_c = 1.160$ gcm⁻³, $\mu(\text{Mo-K}\alpha) = 2.496$ mm⁻¹, $F(000) = 4120$, $T = 298$ K. An orange crystal of dimensions 0.39 mm x 0.28 mm x 0.11 mm mounted in a glass capillary was used for data collection. A total of 40223 unique reflections was obtained from a total of 66025 reflections ($R_{\text{int}} = 0.0355$). According to the SHELXL-97

program,^[S9] 20735 reflections larger than $4\sigma(F_o)$ from a total 40223 reflections were participated in the full-matrix least-squares refinement against F^2 . Convergence for 1689 variable parameters by least-squares refinement on F^2 reaches to $R_1 = 0.0626$ and $wR_2 = 0.1833$ with a goodness-of-fit of 1.086.

Physical Measurements and Instrumentation.

¹H NMR spectra were recorded on a Bruker AVANCE 400 (400 MHz) Fourier-transform NMR spectrometer with chemical shifts reported relative to tetramethylsilane, (CH₃)₄Si. Positive-ion FAB and EI mass spectra were recorded on a Thermo Scientific DFS high resolution magnetic sector mass spectrometer. ESI mass spectra were recorded on a Finnigan LCQ mass spectrometer. Elemental analyses of complexes were performed on a Flash EA 1112 elemental analyzer at the Institute of Chemistry, Chinese Academy of Sciences. The UV-visible spectra were obtained using a Hewlett-Packard 8452A diode array spectrophotometer. Steady-state excitation and emission spectra at room temperature were recorded on a Spex Fluorolog-3 model FL3-211 fluorescence spectrofluorometer equipped with an R2658P PMT detector. Variable-temperature UV-vis absorption spectra were obtained using a Varian Cary 50 UV-vis spectrophotometer. Emission lifetime measurements were performed using a conventional laser system. The excitation source used was the 355-nm output (third harmonic) of a Spectra-Physics Quanta-Ray Q-switched GCR-150-10 pulsed Nd:YAG laser. Luminescence decay signals were detected by a Hamamatsu R928 PMT, recorded on a Tektronix model TDS-620A (500 MHz, 2 GS/s) digital oscilloscope, and analyzed using a program for exponential fits. All solutions for emission lifetime studies were degassed on a high-vacuum line in a two-compartment cell consisting of a 10-mL Pyrex bulb and a 1-cm path length quartz cuvette and sealed from the atmosphere by a Bibby Rotaflo HP6 Teflon stopper. The solutions were rigorously degassed with at least four successive freeze-pump-thaw cycles.

Binding Constant Determination

The electronic absorption spectral titration for binding constant determination was performed in CH₂Cl₂ solution at 25°C with the typical concentration range from 5.0×10⁻⁵ M – 5.0×10⁻⁶ M. Each titration study was conducted at least twice and the results show good reproducibility. Binding constants for 1:1 association were obtained by a nonlinear least-squares fit^[S10] of the absorbance (*A*) vs the concentration of guest added (*C_A*) according to the following equation:

$$A = A_0 + \frac{A_{lim} - A_0}{2C_0} [C_0 + C_A + 1/K_S - [(C_0 + C_A + 1/K_S)^2 - 4C_0C_A]^{1/2}] \quad (1)$$

where *A*₀ and *A* are the absorbance of the host at a selected wavelength in the absence and presence of the guest, respectively, [*C*₀] is the total concentration of the host, [*C_A*] is the concentration of the guest, *A*_{lim} is the limiting value of absorbance in the presence of excess guest, and *K_S* is the binding constant.

For emission titration studies, Eq. 1 can be modified to give Eq. 2, written as

$$I = I_0 + \frac{I_{lim} - I_0}{2C_0} [C_0 + C_A + 1/K_S - [(C_0 + C_A + 1/K_S)^2 - 4C_0C_A]^{1/2}] \quad (2)$$

where *I*₀ and *I* are the emission intensities of the complex at a selected wavelength in the absence and presence of the ion, respectively, and *I*_{lim} is the limiting value of the emission intensity in the presence of excess guests.

Because the binding constant of the association between **1** and [Pt(C[^]N[^]C)(C≡C-C₆H₄-OMe-*p*)](NBu₄) was quite large, the titration study had to be performed under dilute condition (less than *ca.* 10⁻⁶ M). Due to this limitation, their binding constant could not be determined by UV-vis measurements.

References

- [S1] Lu, W.; Chan, M. C. W.; Cheung, K. K.; Che, C. M. *Organometallics* 2001, **20**, 2477.
- [S2] Berenguer, J. R.; Lalinde, E.; Torroba, J. *Inorg. Chem.* 2007, **46**, 9919.
- [S3] Zhou, X. Y.; Kostic, N. M. *Inorg. Chem.* 1988, **27**, 4402.
- [S4] Zhao, L.; Wong, K. M. C.; Li, B.; Li, W.; Zhu, N.; Wu, L.; Yam, V. W. W. *Chem.-A Eur. J.* 2010, **16**, 6797.
- [S5] Abu-salah, O. M.; Al-Ohaly, A. R.; Al-Qahtani, H. A. *Inorg. Chim. Acta.* 1986, **117**, L29.
- [S6] Wong, K. M. C.; Hung, L.-L.; Lam, W. H.; Zhu, N.; Yam, V. W. W. *J. Am. Chem. Soc.* 2007, **129**, 4350.
- [S7] Souharce, B.; Kudla, C. J.; Forster, M.; Steiger, J. Anselmann, R.; Thiem, H.; Scherf, U. *Macromol. Rapid Commun.* 2009, **30**, 1258.
- [S8] (a) Yip, H. K.; Cheng, L. K.; Cheung, K. K.; Che, C. M. *J. Chem. Soc., Dalton Trans.* 1993, 2933. (b) Buechner, R.; Field, J. S.; Haines, R. J.; Cunningham, C. T.; McMillin, D. R. *Inorg. Chem.* 1997, **36**, 3952.
- [S9] Sheldrick, G. M. *Acta Crystallographica.* 2008, **A64**, 112.
- [S10] Bourson, J.; Pouget, J.; Valeur, B. *J. Phys. Chem.* 1993, **97**, 4552.

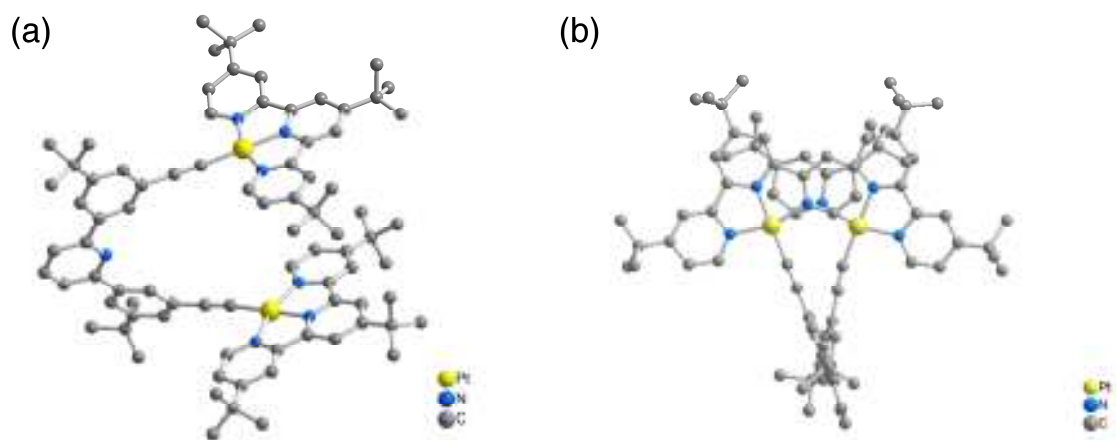


Figure S1. Perspective view of the complex cation of **1** showing the (a) side view and the (b) top view. Hydrogen atoms have been omitted for clarity.

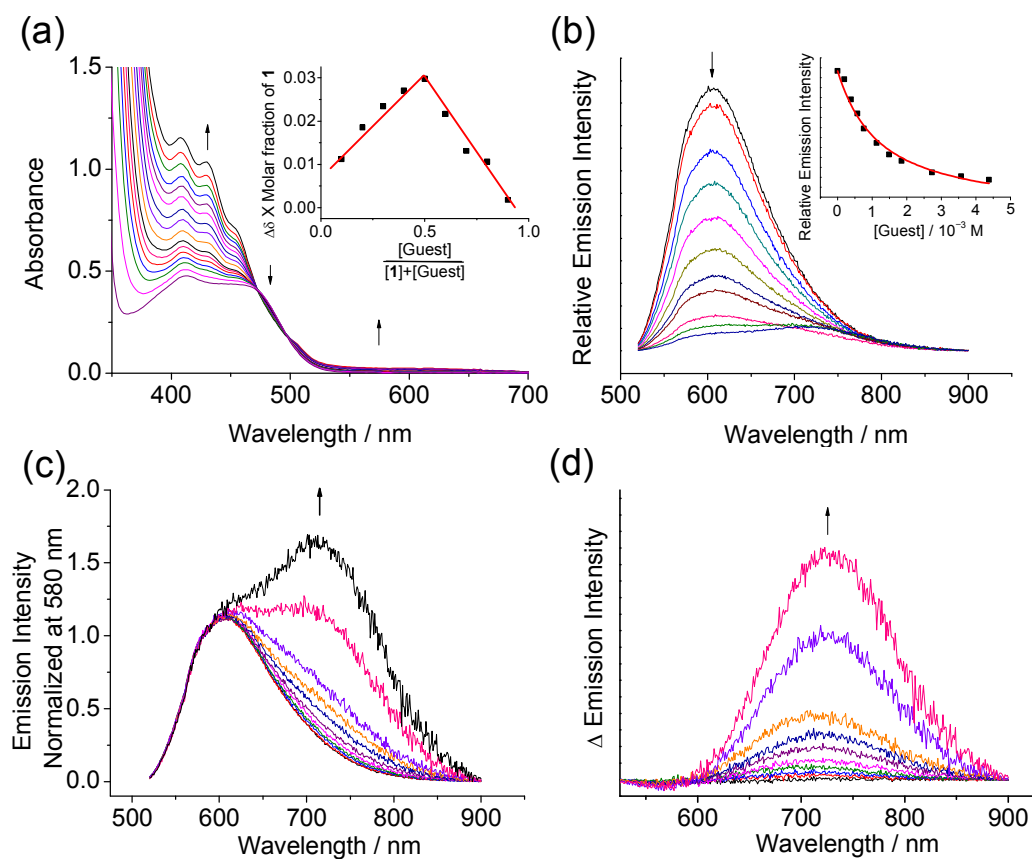


Figure S2. (a) UV-Vis spectral changes of **1** upon addition of $[\text{Pt}(\text{C}^{\wedge}\text{N}^{\wedge}\text{C})(\text{DMSO})]$. Inset shows the Job's plot determined by ^1H NMR study based on pyridine resonances adjacent to Pt. (b) Emission spectral changes of **1** upon addition of $[\text{Pt}(\text{C}^{\wedge}\text{N}^{\wedge}\text{C})(\text{DMSO})]$. Inset shows the emission intensity at 612 nm (\bullet) and its theoretical fit ($—$). (c) Emission spectra of **1** normalized to the band at 580 nm upon addition of $[\text{Pt}(\text{C}^{\wedge}\text{N}^{\wedge}\text{C})(\text{DMSO})]$. (d) Emission difference spectra based on normalized spectra of **1**.

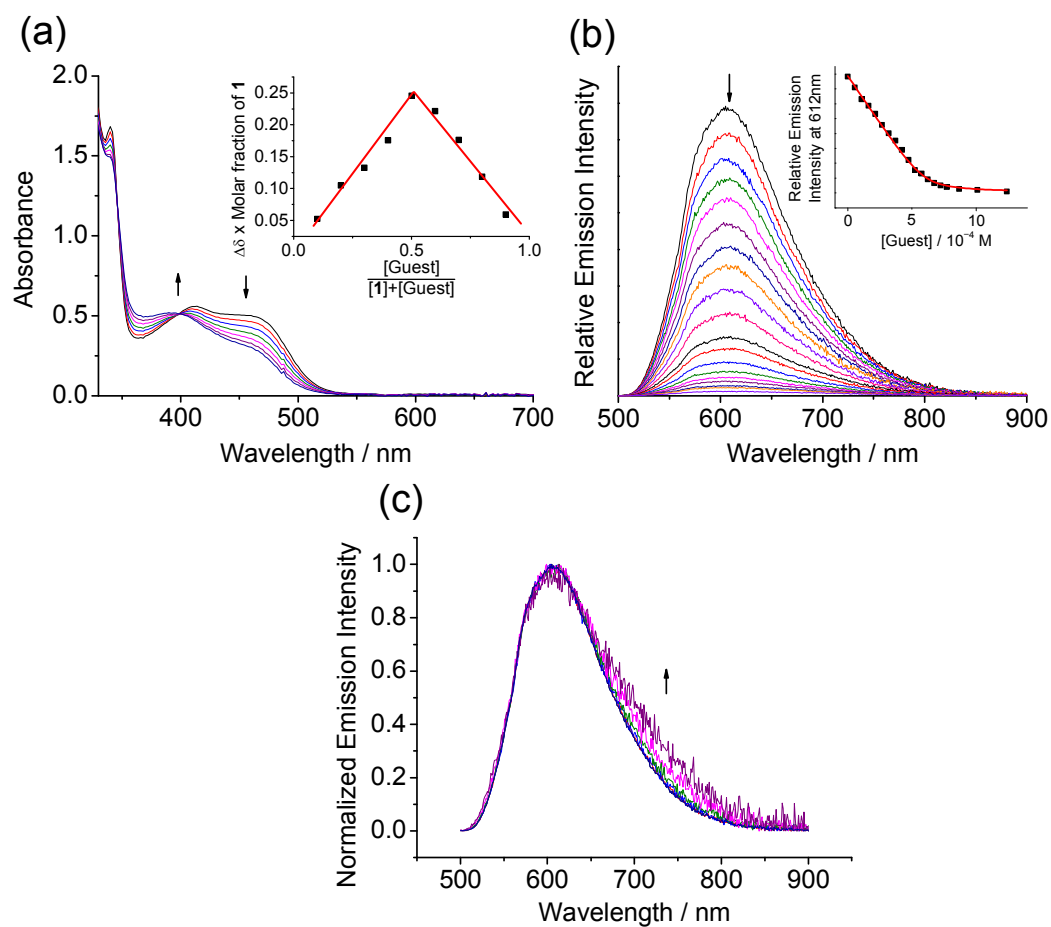


Figure S3. (a) UV-Vis spectral changes of **1** upon addition of $[\text{Pt}(\text{O}^{\wedge}\text{N}^{\wedge}\text{O})\text{Cl}](\text{NBu}_4)$. Inset shows the Job's plot determined by ^1H NMR study based on pyridine resonances adjacent to Pt. (b) Emission spectral changes of **1** upon addition of $[\text{Pt}(\text{O}^{\wedge}\text{N}^{\wedge}\text{O})\text{Cl}](\text{NBu}_4)$. Inset shows the plot of emission intensity at 612 nm (\bullet) and its theoretical fit ($—$). (c) Normalized emission spectra of **1** upon addition of $[\text{Pt}(\text{O}^{\wedge}\text{N}^{\wedge}\text{O})\text{Cl}](\text{NBu}_4)$.

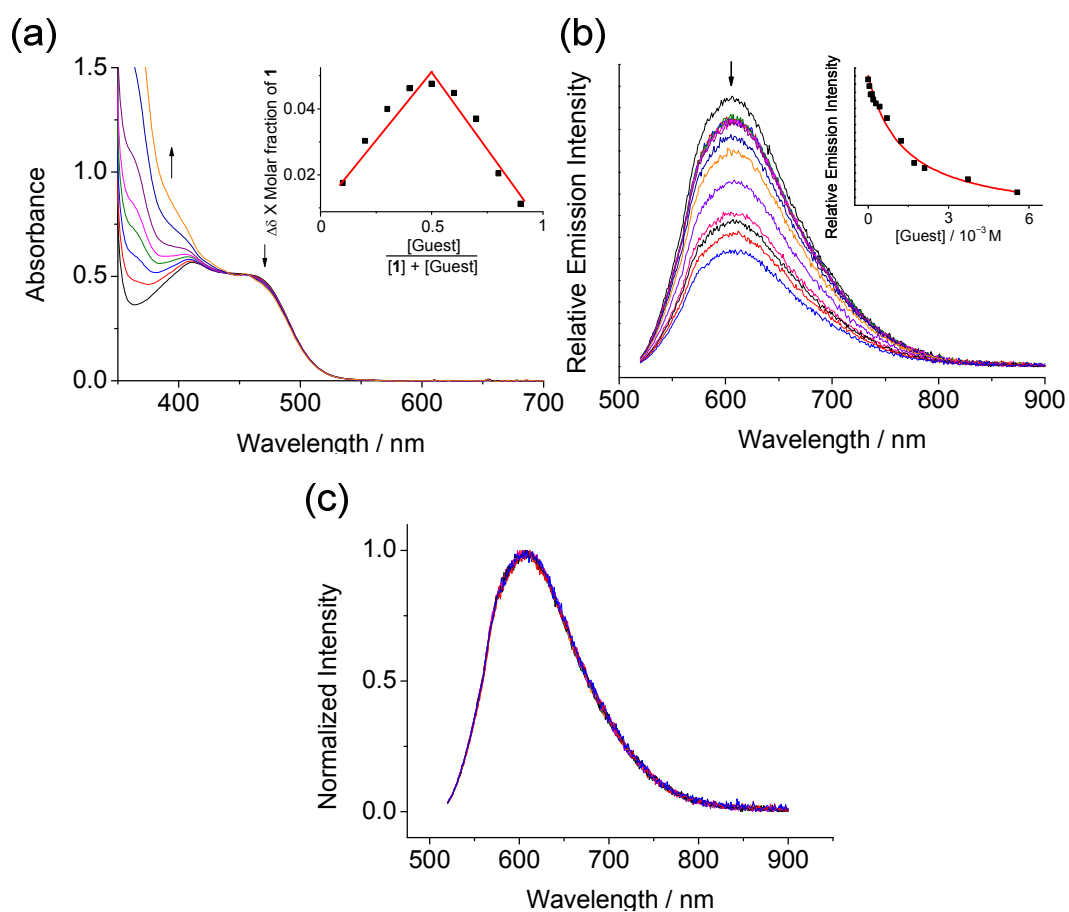


Figure S4. (a) UV-Vis spectral changes of **1** upon addition of $[\text{Pt}(\text{N}5\text{C}12)\text{Cl}]\text{PF}_6$. Inset shows the plot of absorbance at 480 nm. (b) Emission spectral changes of **1** upon addition of $[\text{Pt}(\text{N}5\text{C}12)\text{Cl}]\text{PF}_6$. Inset shows the emission intensity at 612 nm (\bullet) and its theoretical fit (—). (c) Normalized emission spectra of **1** upon addition of $[\text{Pt}(\text{N}5\text{C}12)\text{Cl}](\text{PF}_6)$.

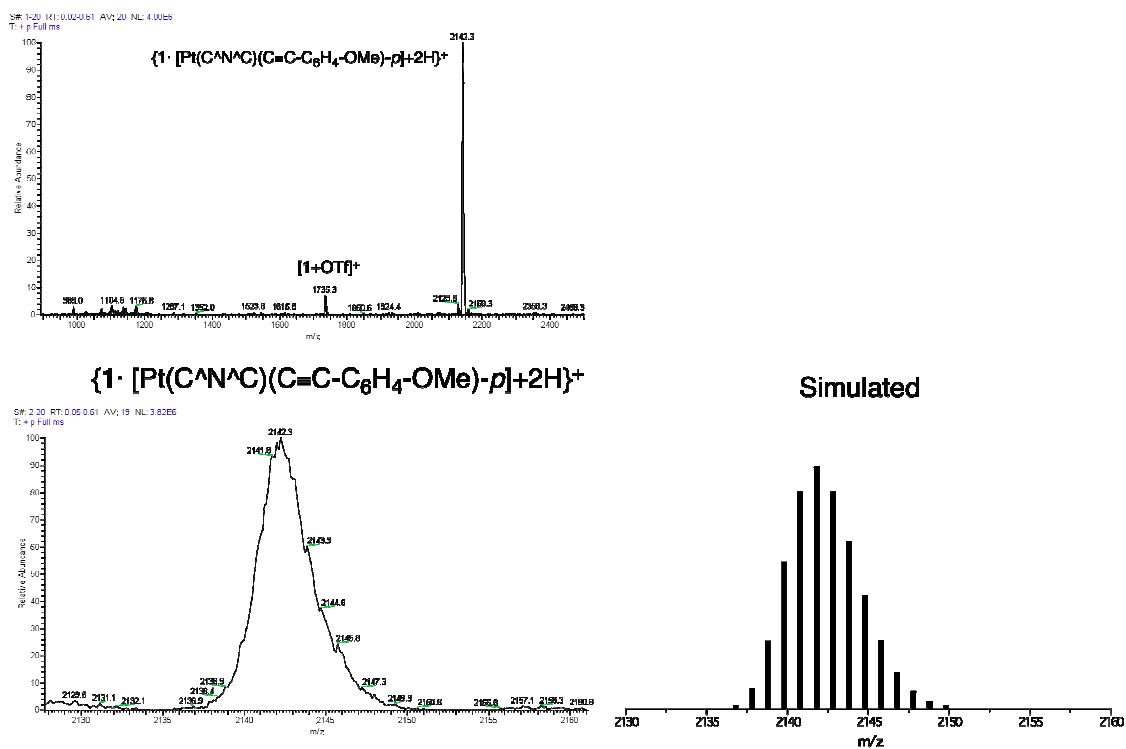


Figure S5. Positive ESI-mass spectrum of **1** in the presence of $[\text{Pt}(\text{C}^{\wedge}\text{N}^{\wedge}\text{C})(\text{C}\equiv\text{C}-\text{C}_6\text{H}_4-\text{OMe})-p](\text{NBu}_4)$ and the simulated isotope pattern of $\{1 \cdot [\text{Pt}(\text{C}^{\wedge}\text{N}^{\wedge}\text{C})(\text{C}\equiv\text{C}-\text{C}_6\text{H}_4-\text{OMe})-p]+2\text{H}\}^+$ in CH_2Cl_2 solution.

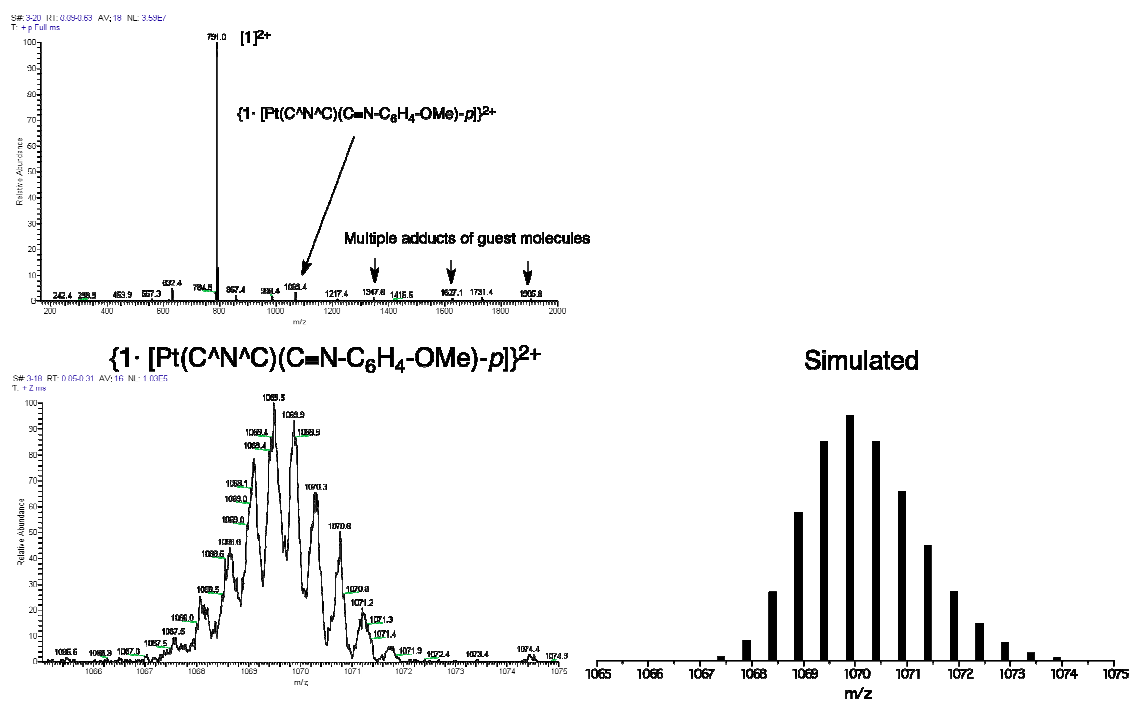


Figure S6. Positive ESI-mass spectrum of **1** in the presence of $[Pt(C^N^C)(C \equiv N-C_6H_4-OMe)-p]$ and the simulated isotope pattern of $\{1 \cdot [Pt(C^N^C)(C \equiv N-C_6H_4-OMe)-p]\}^{2+}$ in CH_2Cl_2 solution.

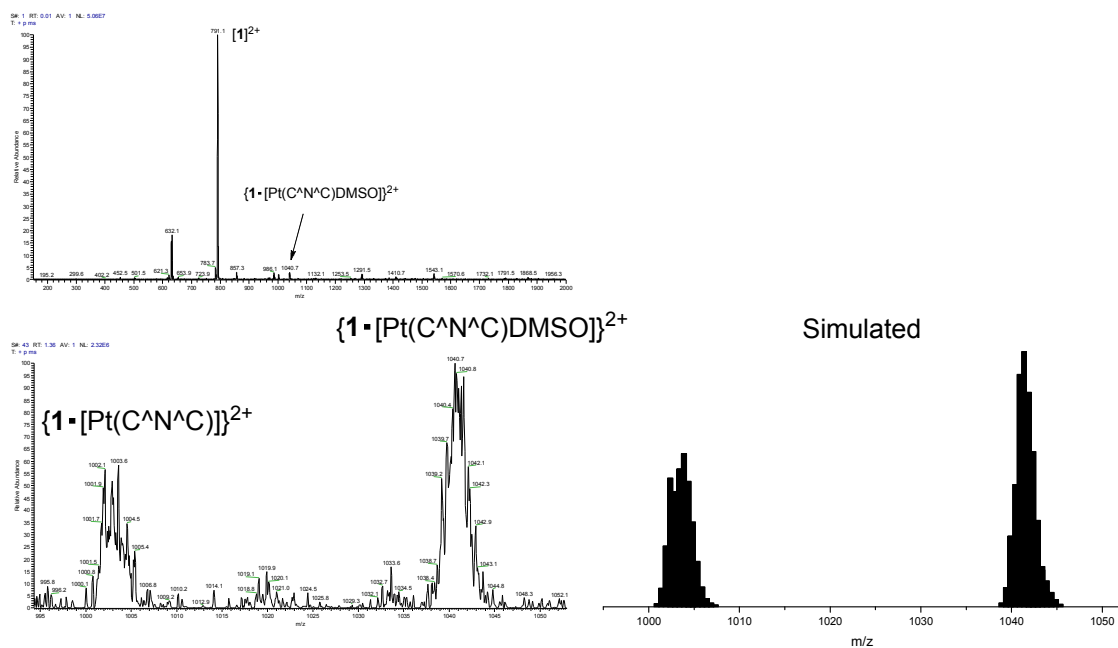


Figure S7. Positive ESI-mass spectrum of **1** in the presence of $[\text{Pt}(\text{C}^{\wedge}\text{N}^{\wedge}\text{C})(\text{DMSO})]$ and the simulated isotope pattern of $\{\mathbf{1}\cdot[\text{Pt}(\text{C}^{\wedge}\text{N}^{\wedge}\text{C})(\text{DMSO})]\}^{2+}$ in CH_2Cl_2 solution.

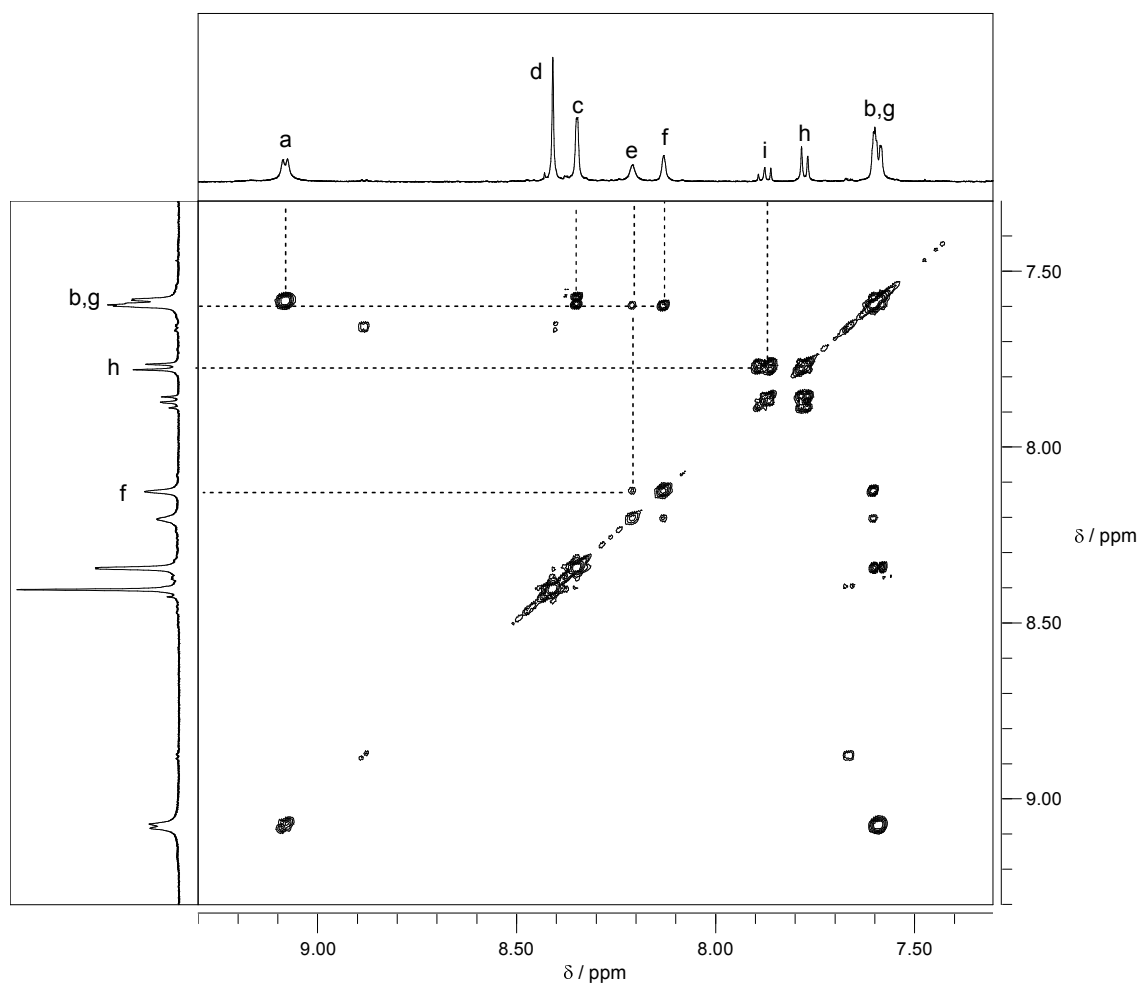


Figure S8. ^1H - ^1H -COSY NMR spectrum of **1** in CDCl_3 at 298 K in the aromatic region.

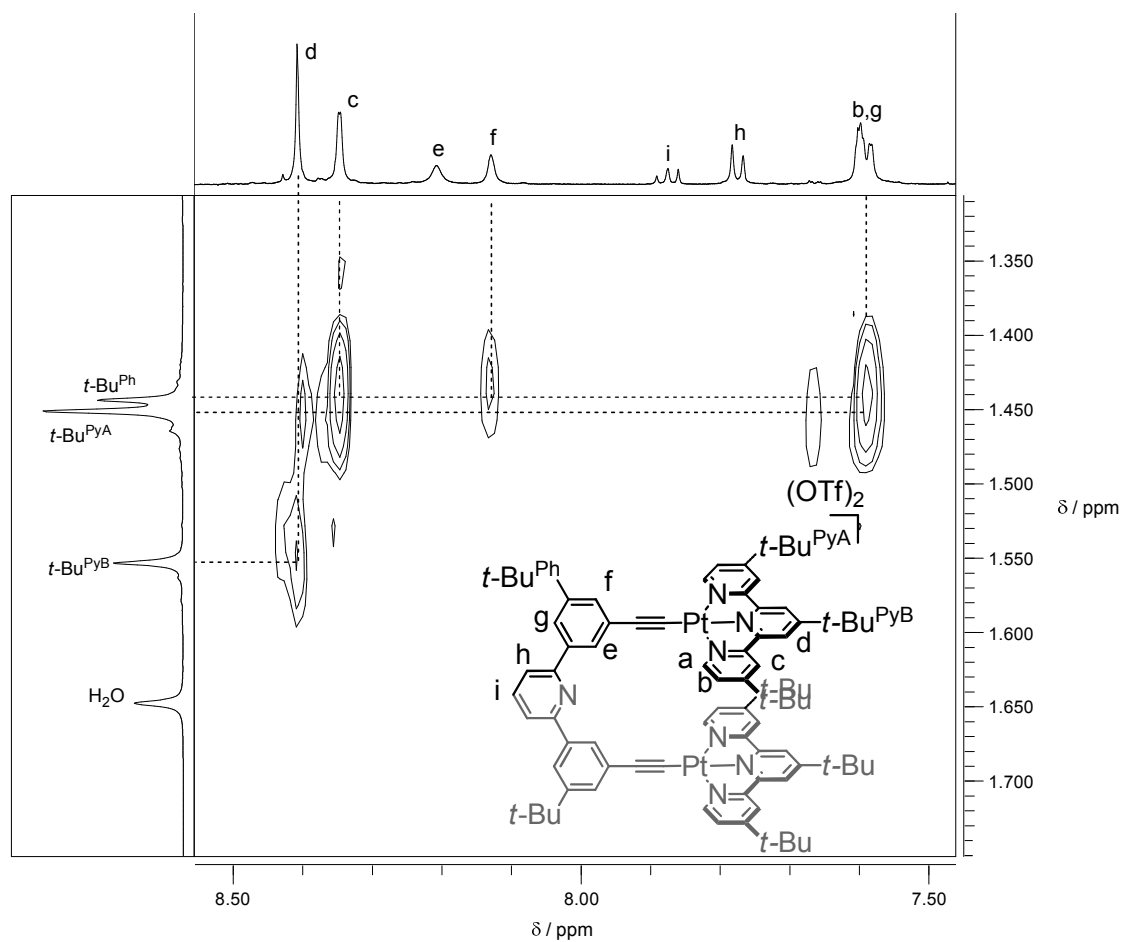


Figure S9. Partial ^1H - ^1H -NOESY NMR spectrum of **1** in CDCl_3 at 298 K.

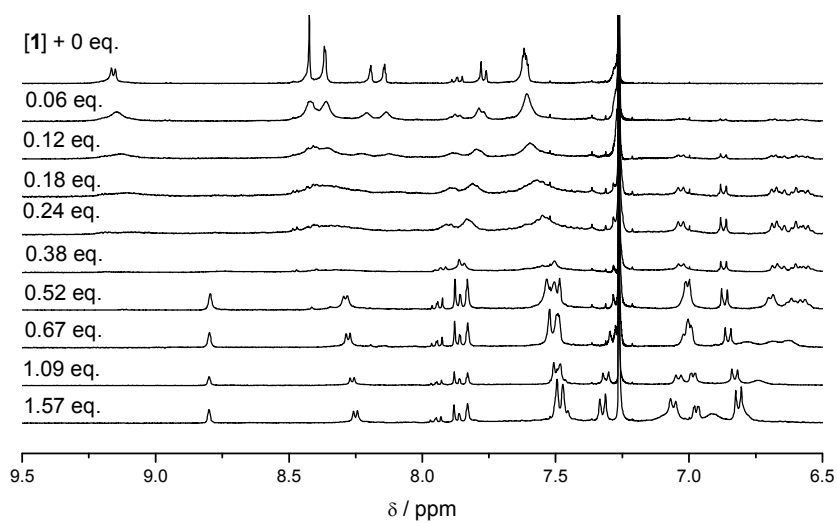


Figure S10. ^1H NMR titration of **1** upon addition of $[\text{Pt}(\text{C}^{\wedge}\text{N}^{\wedge}\text{C})(\text{C}\equiv\text{C}-\text{C}_6\text{H}_4-\text{OMe}-p)](\text{NBu}_4)$ in CDCl_3 solution at 298 K.

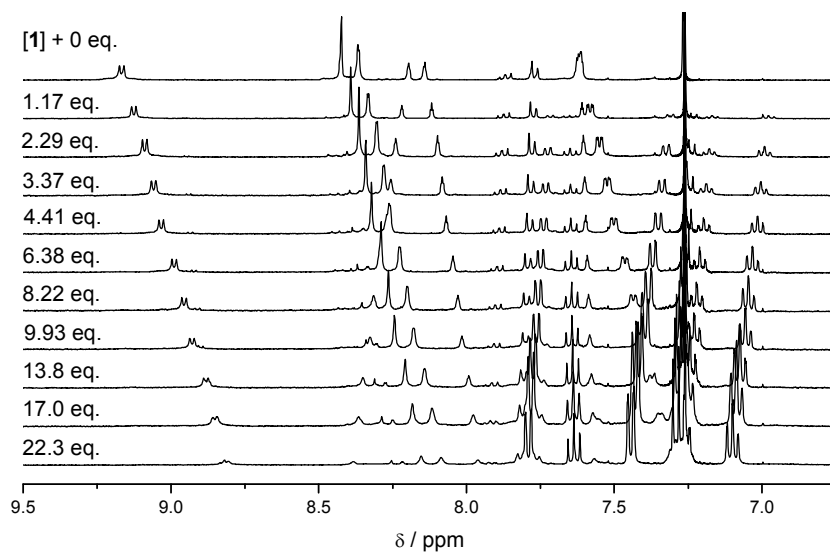


Figure S11. ^1H NMR titration of **1** upon addition of $[\text{Pt}(\text{C}^{\wedge}\text{N}^{\wedge}\text{C})(\text{DMSO})]$ in CDCl_3 solution at 298 K.

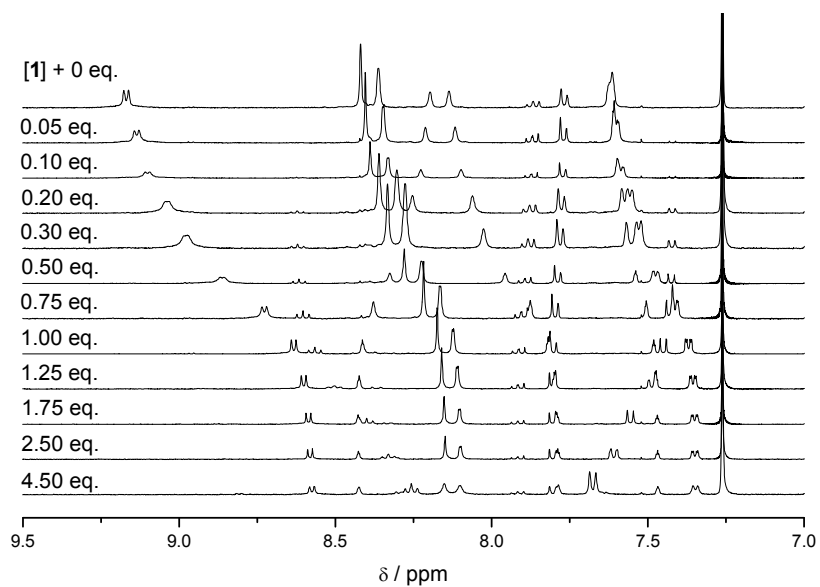


Figure S12. ¹H NMR titration of **1** upon addition of [Pt(O^NO)Cl](NBu₄) in CDCl₃ solution at 298 K.

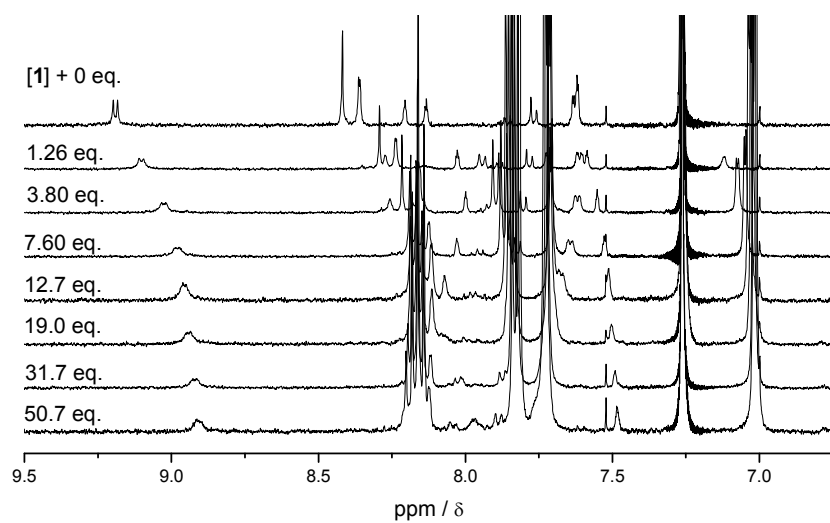


Figure S13. ¹H NMR titration of **1** upon addition of [Pt(N5C12)Cl](PF₆) in CDCl₃ solution at 298 K.

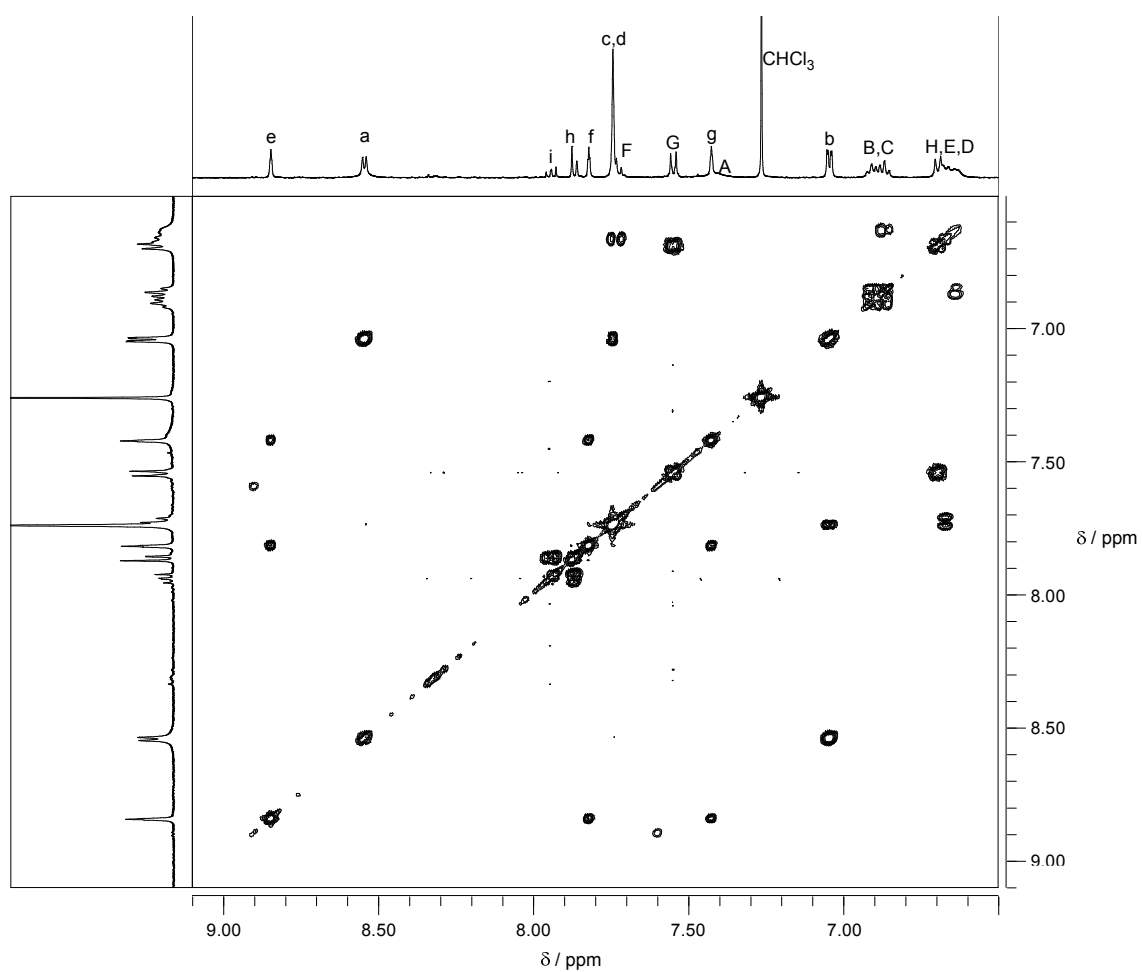


Figure S14. Partial ^1H - ^1H -COSY NMR spectrum of **1** in the presence of 1 equivalent of $[\text{Pt}(\text{C}^{\wedge}\text{N}^{\wedge}\text{C})(\text{C}\equiv\text{N}-\text{C}_6\text{H}_4-\text{OMe}-p)]$ in CDCl_3 at 298 K in the aromatic region.

2D(¹H-¹H-COSY and -NOESY) NMR

¹H-¹H-COSY and -NOESY experiments were also performed for a 1:1 mixture of [Pt(C[^]N[^]C)(C≡N-C₆H₄-OMe-*p*)] and **1** in CDCl₃ solution. For a 1:1 mixture of **1** and the guest, the proton resonance of H_A was broadened and showed an overlap with that of H_G in the guest molecule. Cross-peaks between the proton resonances of H_e in **1** and H_A and H_G of the guest molecule and a cross-peak between H_a in **1** and H_G were observed (Figure S15). Although the observation of cross-peaks for the proton resonances of H_e-H_A in the NOESY experiment (Figure S15) might be a result of the H_g-H_e interaction, the lack of cross-peak intensities between proton resonances of H_e-H_f and H_f-H_g (Figure S16) suggested that the cross-peak indicated in Figure 15 should be mainly responsible for the interaction between H_e and H_A.

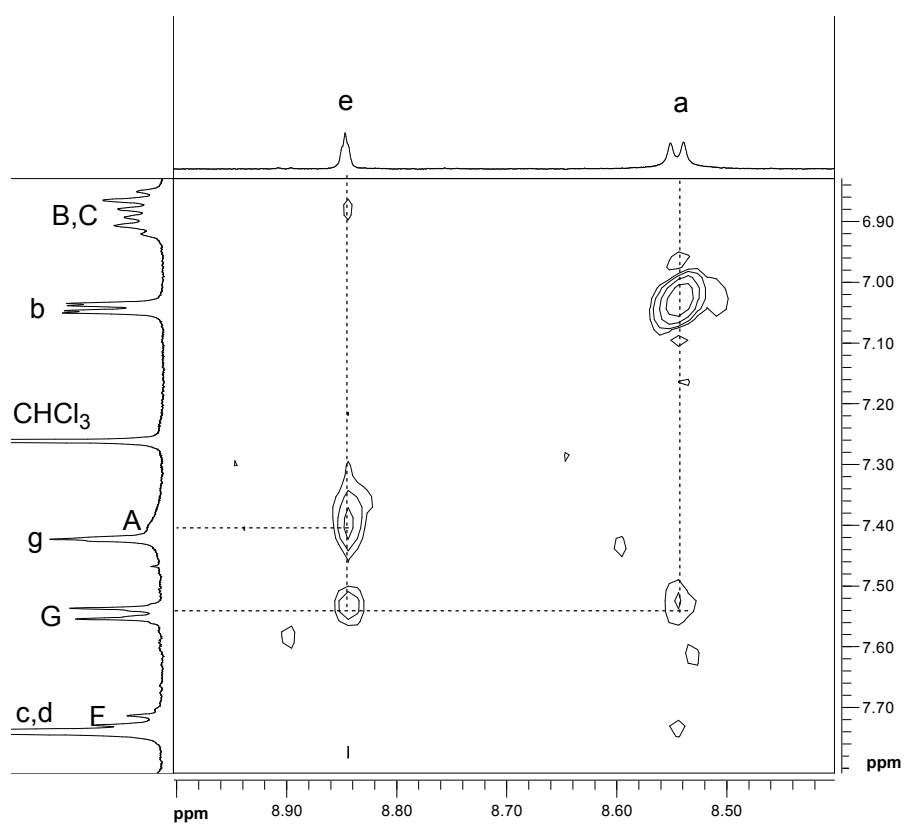


Figure 15. Partial ¹H-¹H-NOESY NMR spectrum of **1** in the presence of 1 equivalent of [Pt(C[^]N[^]C)(C≡N-C₆H₄-OMe-*p*)] in CDCl₃ at 298 K in the aromatic region.

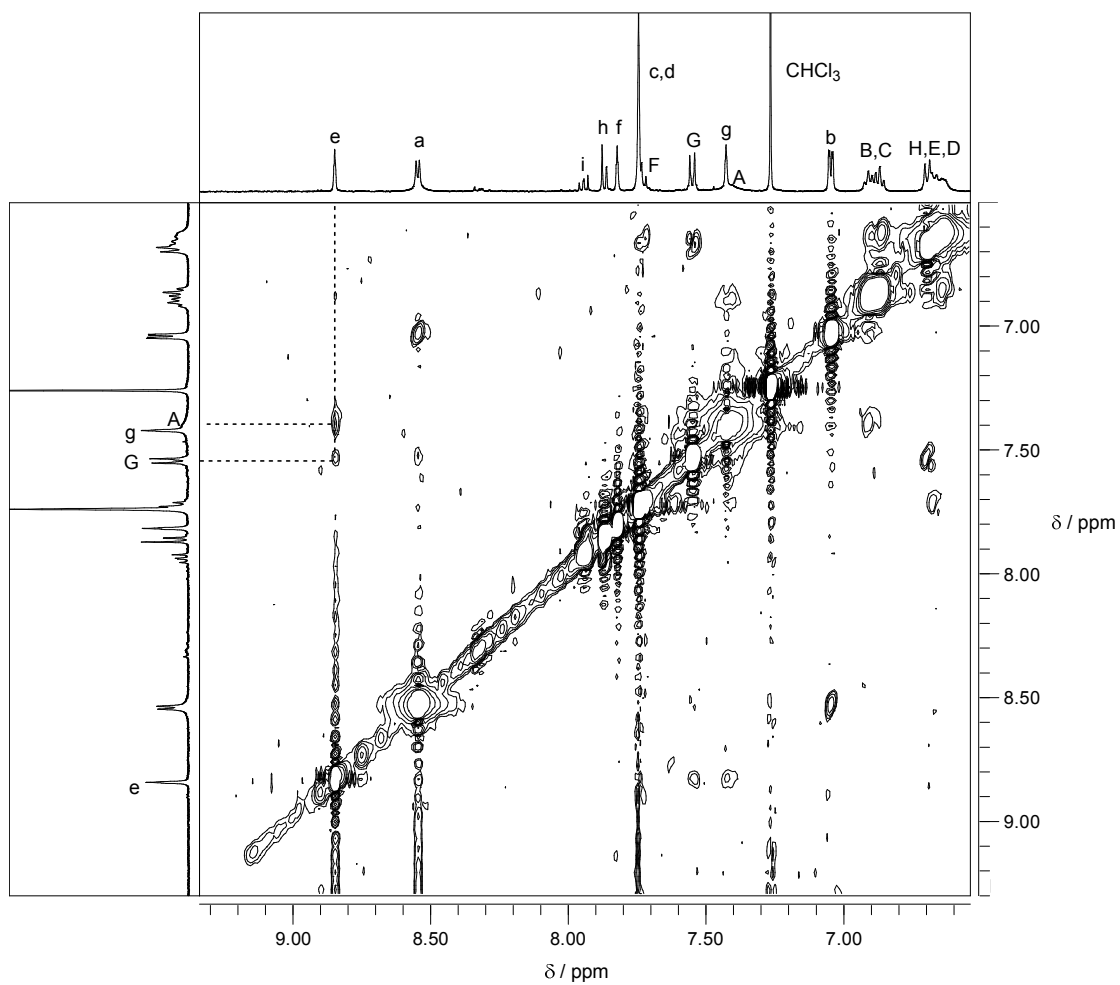


Figure S16. Partial ¹H-¹H-NOESY NMR spectrum of **1** in the presence of 1 equivalent of [Pt(C[^]N[^]C)(C≡N-C₆H₄-OMe-*p*)] in CDCl₃ at 298 K in the aromatic region.

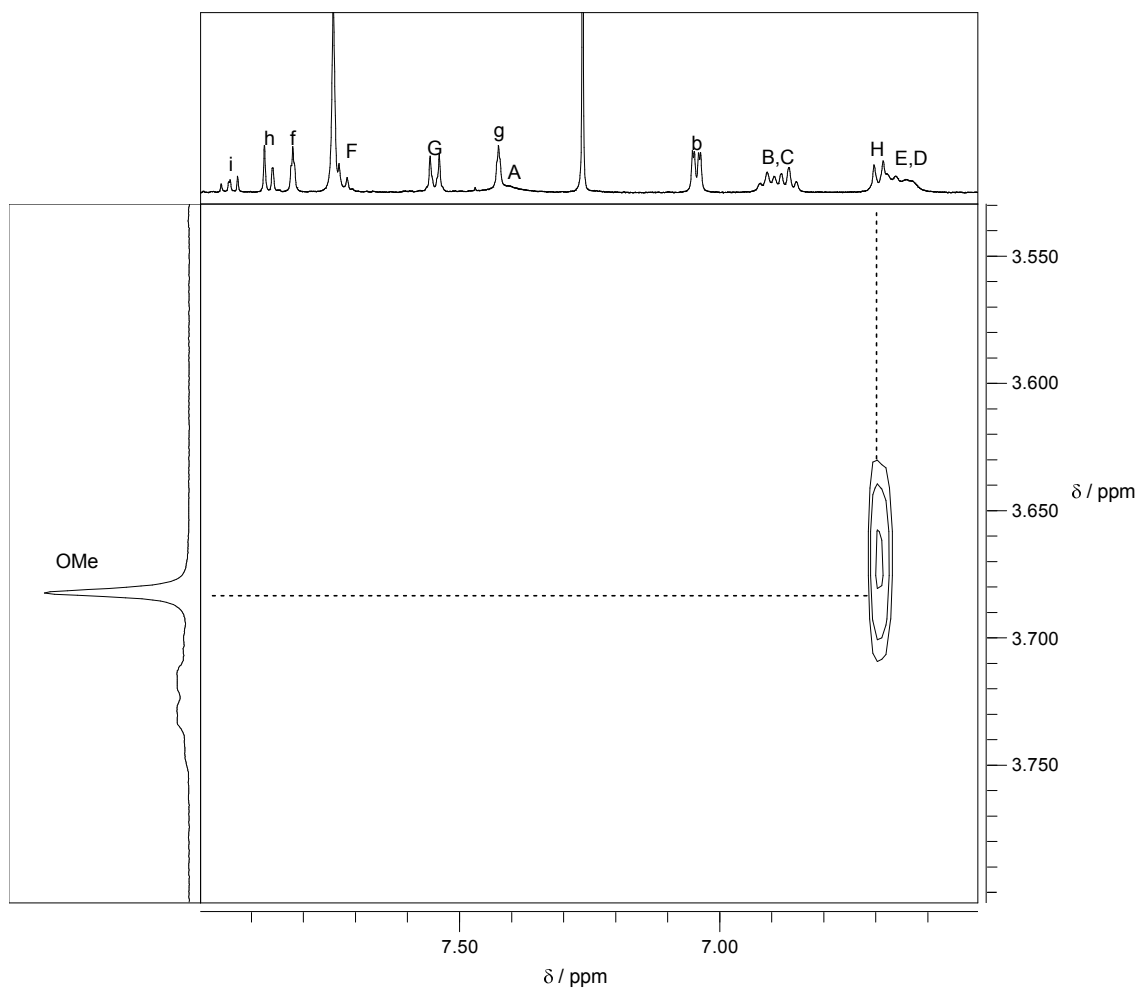


Figure S17. Partial ^1H - ^1H -NOESY NMR spectrum of **1** in the presence of 1 equivalent of $[\text{Pt}(\text{C}^{\wedge}\text{N}^{\wedge}\text{C})(\text{C}\equiv\text{N}-\text{C}_6\text{H}_4-\text{OMe}-p)]$ in CDCl_3 at 298 K in the aromatic region.

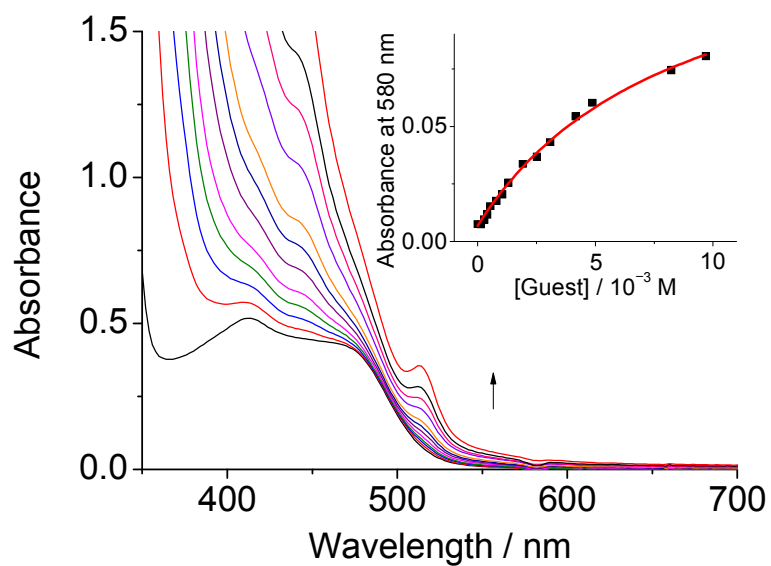


Figure S18. UV-Vis spectral changes of **2** upon addition of $[\text{Pt}(\text{C}^{\wedge}\text{N}^{\wedge}\text{C})(\text{C}\equiv\text{C}-\text{C}_6\text{H}_4-\text{OMe}-p)](\text{NBu}_4)$. Inset shows the plot of absorbance at 600 nm (●) and its theoretical fit (—).

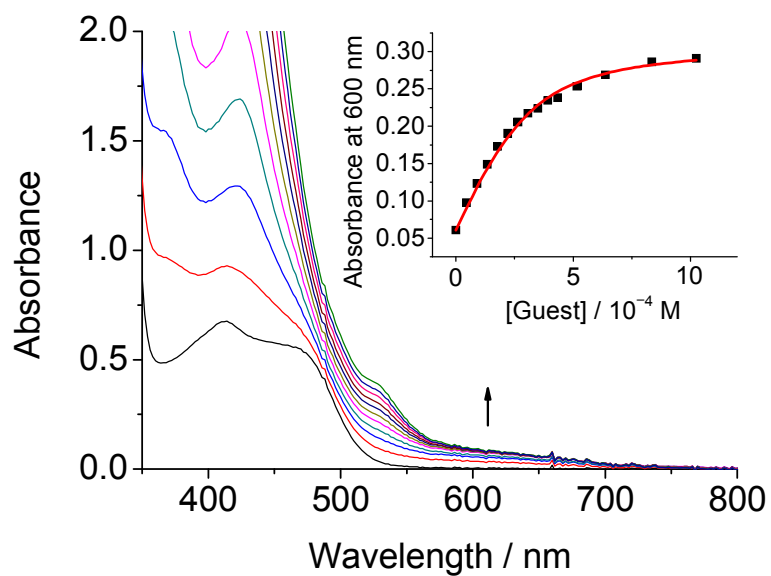


Figure S19. UV-Vis spectral changes of **2** upon addition of [Pt(C[^]N[^]C)(C≡C-C₆H₄-OMe-*p*)](NBu₄). Inset shows the plot of absorbance at 600 nm (●) and its theoretical fit (—).

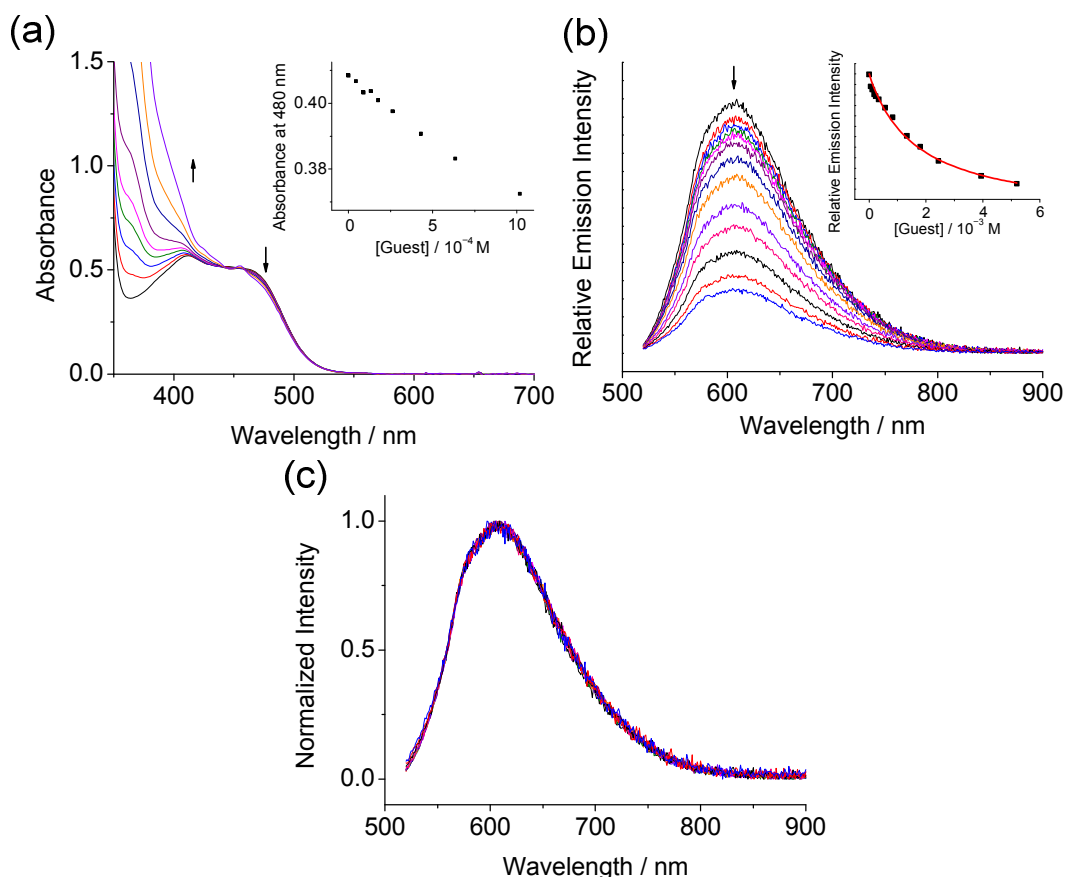


Figure S20. (a) UV-Vis spectral changes of **1** upon addition of $[\text{Pd}(\text{N}5\text{C}12)\text{Cl}]\text{PF}_6$. Inset shows the plot of absorbance at 480 nm. (b) Emission spectral changes of **1** upon addition of $[\text{Pd}(\text{N}5\text{C}12)\text{Cl}]\text{PF}_6$. Inset shows the emission intensity at 612 nm (●) and its theoretical fit (—). (c) Normalized emission spectra of **1** upon addition of $[\text{Pd}(\text{N}5\text{C}12)\text{Cl}]\text{PF}_6$.

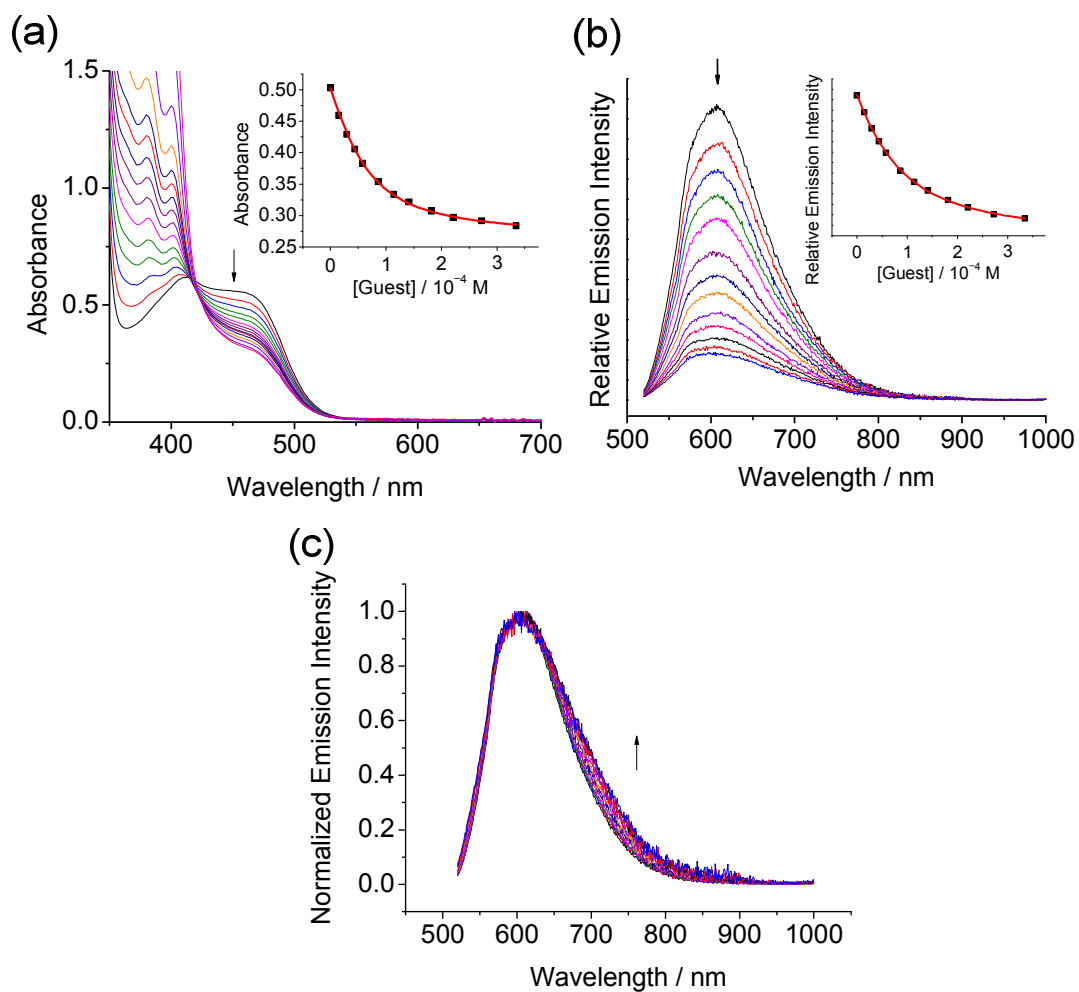


Figure S21. (a) UV-Vis spectral changes of **1** upon addition of $[\text{Au}(\text{C}^{\wedge}\text{N}^{\wedge}\text{C})(\text{C}\equiv\text{C}-\text{C}_6\text{H}_4-\text{OMe})-p]$. Inset shows the emission intensity at 480 nm (●) and its theoretical fit (—). (b) Emission spectral changes of **1** upon addition of $[\text{Au}(\text{C}^{\wedge}\text{N}^{\wedge}\text{C})(\text{C}\equiv\text{C}-\text{C}_6\text{H}_4-\text{OMe})-p]$. Inset shows the emission intensity at 612 nm (●) and its theoretical fit (—). (c) Emission spectra of **1** normalized to the band at 580 nm upon addition of $[\text{Au}(\text{C}^{\wedge}\text{N}^{\wedge}\text{C})(\text{C}\equiv\text{C}-\text{C}_6\text{H}_4-\text{OMe})-p]$.

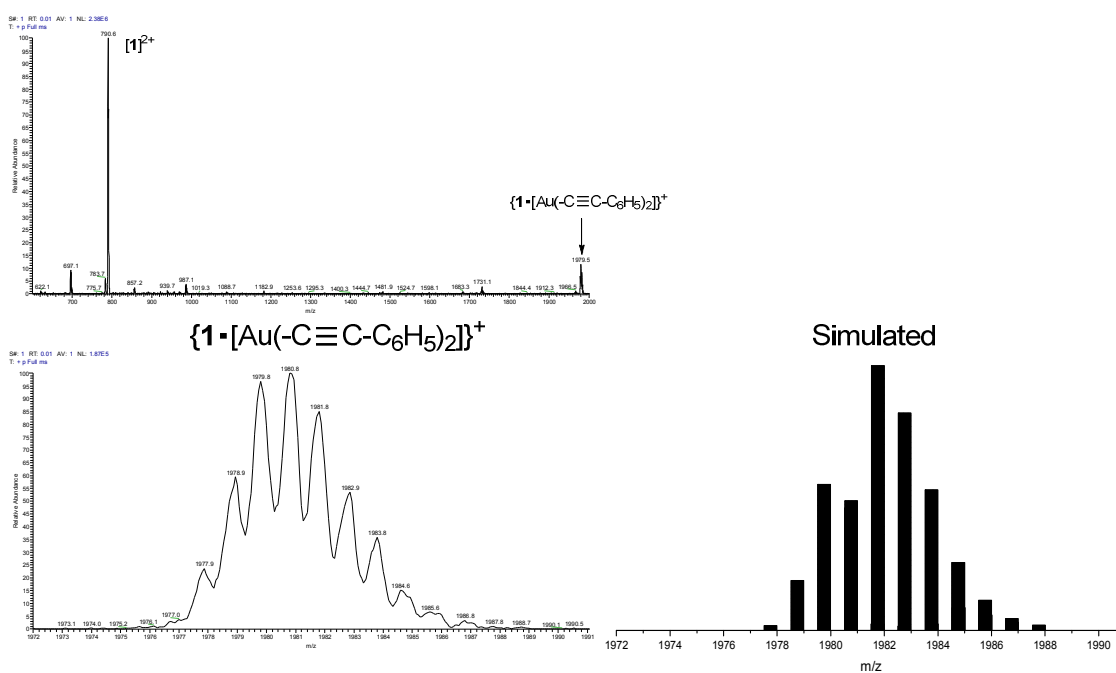


Figure S22. Positive ESI-mass spectrum of **1** in the presence of $[\text{Au}(\text{C}\equiv\text{C}-\text{C}_6\text{H}_5)_2](\text{PPN})$ and the simulated isotope pattern of $\{\mathbf{1}\cdot[\text{Au}(\text{C}\equiv\text{C}-\text{C}_6\text{H}_5)_2]\}^+$ in CH_2Cl_2 solution.

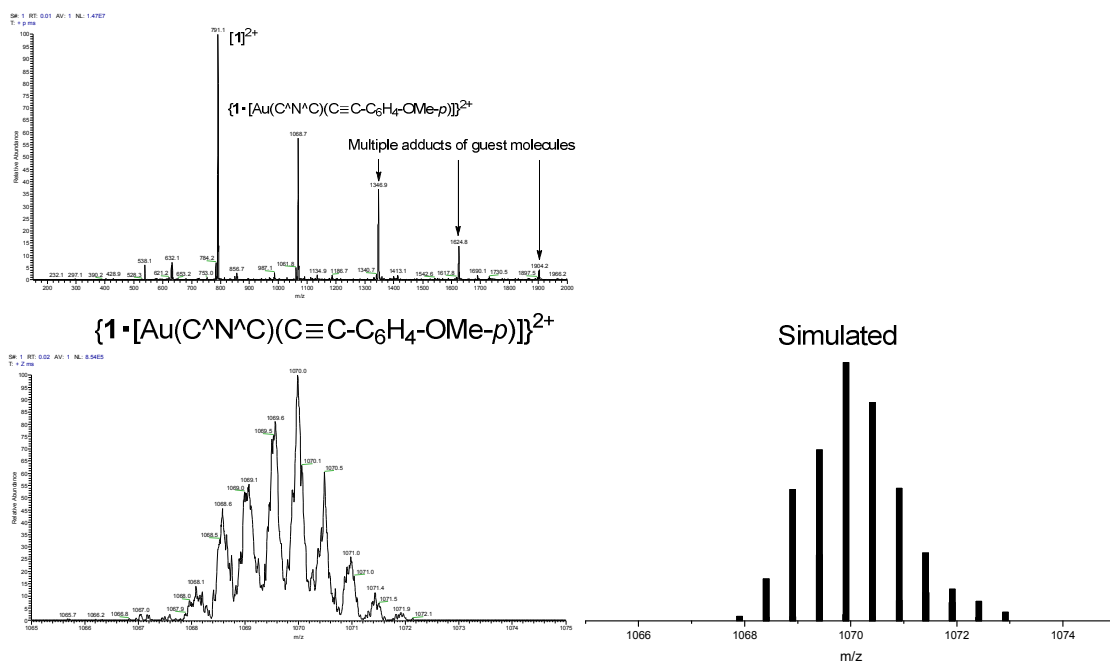


Figure S23. Positive ESI-mass spectrum of **1** in the presence of $[\text{Au}(\text{C}^{\wedge}\text{N}^{\wedge}\text{C})(\text{C}\equiv\text{C}-\text{C}_6\text{H}_4-\text{OMe})-p]$ and the simulated isotope pattern of $\{1 \cdot [\text{Au}(\text{C}^{\wedge}\text{N}^{\wedge}\text{C})(\text{C}\equiv\text{C}-\text{C}_6\text{H}_4-\text{OMe})-p]\}^{2+}$ in CH_2Cl_2 solution.